

Response of closed basin lakes to interannual climate variability

Kathleen Huybers^{1,2} · Summer Rupper^{3,4} · Gerard H. Roe¹

Received: 16 August 2014 / Accepted: 8 August 2015
© Springer-Verlag Berlin Heidelberg 2015

Abstract Lakes are key indicators of a region's hydrological cycle, directly reflecting the basin-wide balance between precipitation and evaporation. Lake-level records are therefore valuable repositories of climate history. However, the interpretation of such records is not necessarily straightforward. Lakes act as integrators of the year-to-year fluctuations in precipitation and evaporation that occur even in a constant climate. Therefore lake levels can exhibit natural, unforced fluctuations that persist on timescales of decades or more. This behavior is important to account for when distinguishing between true climate change and interannual variability as the cause of past lake-level fluctuations. We demonstrate the operation of this general principle for the particular case-study of the Great Salt Lake, which has long historical lake-level and climatological records. We employ both full water-balance and linear models. Both models capture the timing and size of the lake's historical variations.

We then model the lake's response to much longer synthetic time series of precipitation and evaporation calibrated to the observations, and compare the magnitude and frequency of the modeled response to the Great Salt Lake's historical record. We find that interannual climate variability alone can explain much of the decadal-to-centennial variations in the lake-level record. Further, analytic solutions to the linear model capture much of the full model's behavior, but fail to predict the most extreme lake-level variations. We then apply the models to other lake geometries, and evaluate how the timing and amplitude of a lake-level response differs with climatic and geometric setting. A lake's response to a true climatic shift can only be understood in the context of these expected persistent lake-level variations. On the basis of these results, we speculate that lake response to interannual climate variability may play an important part in explaining much of Holocene lake-level fluctuations.

✉ Kathleen Huybers
huyberkm@plu.edu

Summer Rupper
summer_rupper@byu.edu; summer.rupper@geog.utah.edu

Gerard H. Roe
gerard@ess.washington.edu

¹ Department of Earth and Space Sciences, University of Washington, 4000 15th Ave NE, Box 351310, Seattle, WA 98195, USA

² Present Address: Departments of Geosciences and Environmental Studies, Pacific Lutheran University, Rieke Room 158, Tacoma, WA 98447, USA

³ Department of Geological Sciences, Brigham Young University, S389 ESC, Provo, UT 84602, USA

⁴ Present Address: Geography Department, University of Utah, 260 Central Campus Dr Rm 270, Salt Lake City, UT 84112, USA

Keywords Lake-level variability · Lake modeling · Climate variability · Great Salt Lake

1 Introduction

Lakes are important archives of climate history, responding sensitively to variations in evaporation and precipitation. A lake integrates climatic information over its entire catchment area, reflecting regional climate signals with a simple volumetric response. Langbein (1961) noted that closed-basin lakes, which are found in semi-arid regions and lack drainage outlets, fluctuate more than open lakes, because variations in the inflow can only be compensated by a change in the lake's surface area. Therefore, closed lakes are particularly sensitive to climate fluctuations, and have been the subject of many paleoclimate studies (see

Street-Perrott and Harrison 1985; Kohfeld and Harrison 2000).

The integrative nature of lakes also complicates the interpretation of a region's climatic history. A lake proxy record does not distinguish between an increase in precipitation and a decrease in evaporation. Moreover, lakes act as low-pass temporal filters of the climate (e.g. Mason et al. 1994; Liu and Schwartz 2014). For example, if a lake that is initially in steady state experiences a spike in precipitation, its level rises and spatial extent increases. With a larger surface area, the net evaporation also increases, and the lake gradually lowers and returns to its original size. The size and shape of the lake, and the mean climatic state determine the time it takes to return to equilibrium (e.g. Mason et al. 1994). This delayed and smoothed response to a climate signal is a hallmark of other geophysical systems with memory such as the ocean's mixed layer (Hasselmann 1976; Frankignoul and Hasselmann 1977) and glaciers (Oerlemans 2000; Roe 2011). In terms of lakes, both the spatial and temporal integration of evaporation and precipitation can complicate the attribution of a lake-level change to a single climatic event.

The basic mechanism of how a lake re-establishes equilibrium in response to a climate perturbation has been well described in other studies (e.g. Langbein 1961; Mason et al. 1994; Sene 1998; Kohfeld and Harrison 2000; Liu and Schwartz 2014). The specific goal of the present study is to evaluate its implications for the lake-level response to the year-to-year stochastic fluctuations in precipitation and evaporation that occur even in a constant climate. Much of this variability is essentially due to the random vagaries of the weather, and has no interannual or large-scale

persistence (e.g., see Burke and Roe 2014 for a recent discussion and some relevant references). Much of the paleoclimate literature has interpreted lake-level records as reflecting climate changes and variations (see Street-Perrott and Harrison 1985; Bartlein et al. 1998), but has overlooked the possible role of stochastic variability in a constant climate. A parallel series of studies has evaluated the role of stochastic variability for glacier-length fluctuations (e.g. Oerlemans 2000; Roe and O'Neal 2009; Roe and Baker 2014). Such studies show how century-scale, kilometer-scale glacier-length fluctuations should be expected to occur even in a constant climate. Stochastic variability is thus an alternative explanation to climate change that must be considered for many of the Holocene glacial moraines. The present study explores such ideas, but for the different physical system of closed-basin lakes.

Our approach is two-fold. Firstly, we make a detailed case-study of the Great Salt Lake (GSL), where we can take advantage of a large amount of observational data and previous studies. For the GSL we present a full water-balance model and a linear model, calibrated to observations and validated against historical lake measurements. Importantly, the linear model allows for analytic solutions to some key lake metrics, such as the lake-level response time, variance, power spectrum, and the expected return-time of a given lake level, that characterize the lake-level response to interannual climate variability. We evaluate these solutions by driving the lake models with long synthetic climate time series, with variability equal to modern instrumental observations of precipitation and evaporation. Secondly, we apply the findings from the case study in the first part to three distinctly shaped lake-basin geometries.

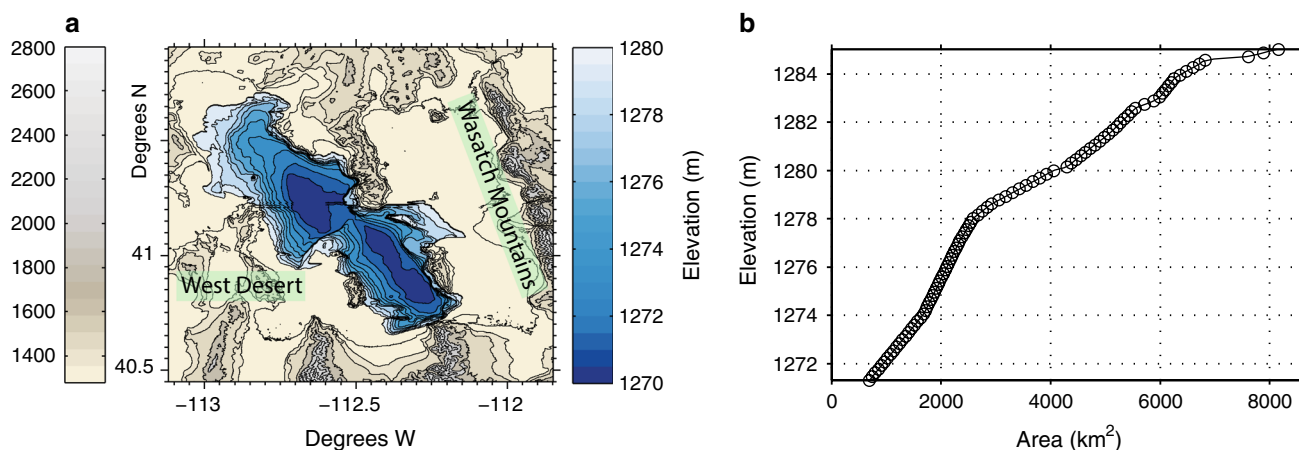


Fig. 1 Great Salt Lake's setting and geometry. **a** Map view of the GSL. Data from Baskin (2005, 2006). Lake levels are contoured every meter. For visual clarity, the surrounding topography is contoured every 20 m from 1280 to 1300 m a.s.l., every 100 m from 1300 to 1500 m a.s.l., and every 300 m from 1500 to 3000 m a.s.l.

b GSL's hypsometric curve from Loving et al. (2000). The present-day lake level is 1279 m a.s.l. which corresponds to a surface area of ~ 3500 km², and is slightly below the historical mean lake level of 1280.4 m a.s.l.

The divergent responses of the different geometries highlight the importance of understanding how a lake's unique geometry and mean climatic state integrates the regional climate history.

2 Case-study setting: the Great Salt Lake

The GSL is located northwest of Salt Lake City, Utah, USA. It is bounded by the West Desert to the west, the Wasatch Range to the east, and is one of the largest terminal lakes in the world, with a surface area averaging 4300 km² (including evaporation ponds for mineral recovery) over the past 166 years (see Fig. 1a). The GSL is filled predominantly by inflow from surrounding rivers (66 %) and direct precipitation (31 %), with groundwater accounting for the small balance of the input (Arnow 1985). Water is lost primarily through evaporation. Despite its vast area, the lake is quite shallow, with a maximum depth of ~10 m (e.g. Arnow and Stephens 1990). This aspect ratio is summarized in the lake's hypsometry (Fig. 1b, taken from Loving et al. (2000)). These dimensions mean that even a small imbalance between inflow and outflow can drive large changes in lake area.

The GSL has a long historical record of lake level (Fig. 2a). From 1847–1874, lake levels were estimated by observing the water depth over sandbars in the lake (Arnow and Stephens 1990). Since 1875, the United States Geological Survey (USGS) has been collecting water-surface elevation data directly. After linearly detrending the time series of interannual lake level, the standard deviation is 1.14 m. We will characterize lake level by the elevation of the lake surface above sea level (a.s.l.). Over the historical record, the average lake level has been 1280.4 m a.s.l. The record low, in 1963, was 1277.5 m a.s.l., corresponding to a maximum depth of 8 m and a surface area of ~2500 km². In contrast, the lake's historical high in 1987 of 1283.8 m a.s.l. corresponds to a depth of 14 m, and a surface area of ~6200 km². This high stand required an expensive pumping project to relocate the excess water (Loving et al. 2000). Thus, lake area has varied by a factor of approximately 2.5 over the historical record.

2.1 Climate: precipitation

The catchment basin of the GSL is large (5.5×10^4 km²) and topographically varied, so a single rain gauge does not reflect the entire basin's precipitation. Given sparse, and sometimes noncontinuous records, there will be some uncertainty in the precipitation history. For this work, we choose to use the University of Delaware's monthly gridded precipitation product, which provides a continuous record from 1900 to 2010, based on an interpolation onto a 0.5° by 0.5° latitude/longitude grid

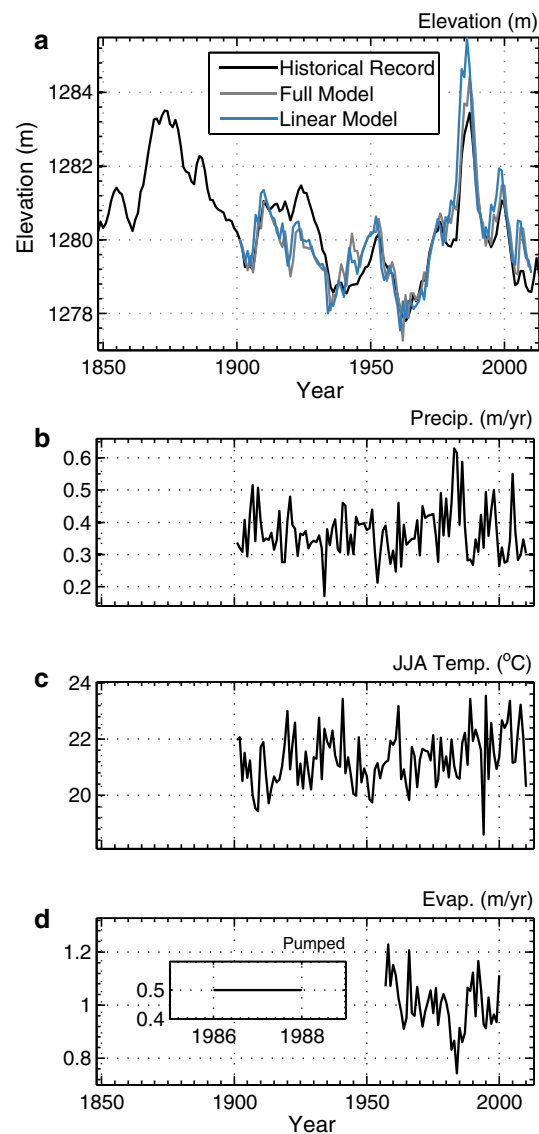


Fig. 2 GSL's lake level and climatological history. **a** The historical record of the GSL, from USGS Water Resources (2013), is shown in *black*. The *grey* and *blue* lines show the full and linear output from the modeled history, respectively. The models incorporate the precipitation and evaporation data from **b** and **d**. **b** Annual regional precipitation record, from Matsuura and Willmott (2012). Precipitation is summed over the water-year, from October to September. **c** Mean regional summer (JJA) temperatures from Willmott et al. (2012). **d** Compilation of evaporation records from local pan measurements, from Western Regional Climate Center (2013). The inset shows the approximate annual volume of water pumped from the lake in 1986–1988, divided by the lake's area, so that this rate of removal is comparable to the evaporation rate

(Matsuura and Willmott 2012). We sum the monthly totals into an annual record based on the water year, from October to September (Arnow 1985; Arnow and Stephens 1990) (Fig. 2b). Based on this data set, the mean (μ_P) and standard deviation (σ_P) in precipitation for the GSL basin are 0.37 and 0.08 m year⁻¹, respectively.

2.2 Climate: evaporation

Because it is difficult to directly measure, evaporation data is sparse and unreliable. Overlake evaporation is a function of temperature, wind, relative humidity, and salinity (e.g. Morton 1986). Among these variables, only temperature has a long and reliable record. Based on the University of Delaware's gridded monthly temperature data (Willmott et al. 2012), average yearly summer (JJA) 2 m air temperature for the GSL area is 21.3 °C, and the standard deviation in temperature is 0.91 °C (Fig. 2c). In previous studies, evaporation records of the GSL have been derived through mass-balance modeling and a modified Penman-Montieth equation, though each of these has drawbacks (Mohammed and Tarboton 2012). The mass balance approach assumes that all other quantities are perfectly known, while the modified Penman equation may not properly apportion the system's available energy, and is more appropriate for time-scales on the order of a day.

We follow Waddell and Barton (1980), Arnow (1985), and Arnow and Stephens (1990) in estimating overlake evaporation on the basis of nearby pan-evaporation data. We piece together the temporal variations in evaporation using pan-evaporation records from two sites near the GSL: Saltair (1957–1990) and Logan Farm (1971–2000) (data from Western Regional Climate Center 2013, www.wrcc.dri.edu). We align these records, setting the mean to $\mu_E = 1 \text{ m year}^{-1}$, and the standard deviation to $\sigma_E = 0.1 \text{ m year}^{-1}$, in agreement with the water-balance model of Mohammed and Tarboton (2012) (Fig. 2d). Pan-evaporation records are subject to significant uncertainty, but are reasonable, if imperfect estimates of overlake evaporation, capturing the relative changes over time. We will later show that evaporation is of secondary importance to precipitation in driving the GSL's lake-level changes, and so our analysis is not critically dependent on the evaporation record.

2.3 Persistence in the lake and the climate time series

It is clear even visually from Fig. 2 that the time series of precipitation, temperature, and evaporation have much less persistence than that of the lake itself. Persistence can be explicitly quantified by calculating the autocorrelation function of a time-series (Fig. 3). One simple test of whether there is any significant persistence in a time series is whether the lag-1 autocorrelation exceeds $\frac{2}{\sqrt{N}}$, where N is the number of points in the time series (e.g. von Storch and Zwiers 2001). These threshold levels are shown for their respective time series in Fig. 3. Based on this test, we conclude that no significant persistence exists for temperature and evaporation. Some slight interannual persistence may be indicated for the precipitation record, though its significance is marginal.

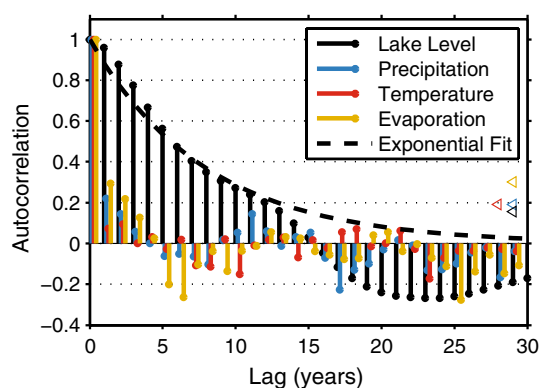


Fig. 3 Autocorrelation function of the GSL's historical lake-level (USGS Water Resources 2013), regional annual precipitation rate (Matsuura and Willmott 2012), regional JJA temperature (Willmott et al. 2012), and evaporation rate (Western Regional Climate Center 2013). The arrows on the right side of the graph indicate the 2σ confidence level of a significant autocorrelation, which is a function of the length of the records. The lake has significant memory up to 13 years, with an e -folding timescale of 8 years. With the exception of precipitation, which exhibits a small autocorrelation of up to a year [using calendar year or water-year average monthly precipitation totals from Matsuura and Willmott (2012)], the climate variables have no significant autocorrelation, indicating that they can be described as white noise processes. The dashed black line displays an exponential function with an e -folding decay time of 8 years

Figure 3 demonstrates that the lake-level fluctuations themselves do exhibit significant persistence, and further, that this persistence is characterized by an exponential fit with a characteristic e -folding timescale, or memory, of approximately 8 years. The exponential fit underestimates the autocorrelation at lags less than five years, a discrepancy which we explore later in this paper. Because there is little to no persistence in the climate variables, the lake's memory must arise from the lake's adjustment rather than being intrinsic to the climate. The main point of the present study is that the lake exhibits memory that is not present in the climate. Analysis of the lake models that we develop below explain much of this behavior.

2.4 Previous research

Prior research has characterized the GSL as a low-order system, and suggests that the lake's volume anomalies slightly lag the regional precipitation and temperature anomalies (Abarbanel and Lall 1996; Abarbanel et al. 1996; Sangoyomi et al. 1996; Lall et al. 1996). Related research invokes low-frequency climate phenomena to explain the low-frequency response of the GSL (Mann et al. 1995; Lall and Mann 1995; Moon et al. 2008; Wang et al. 2010). These studies aim to use some combination of atmospheric indices to predict the GSL lake levels. In this study we aim to put these explanations into context by considering

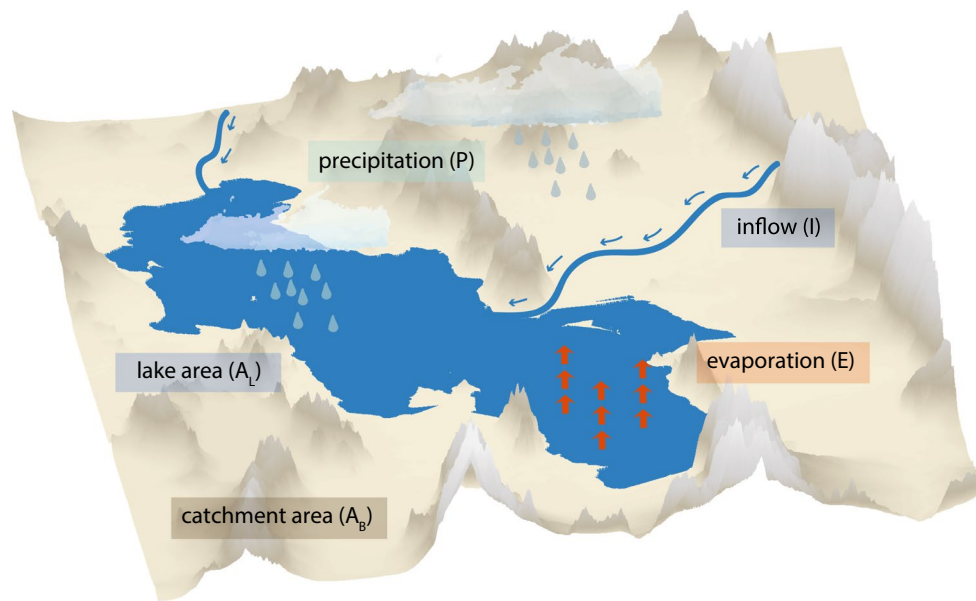


Fig. 4 Schematic of inputs into the full and linear models. The lake gains volume from both direct precipitation into the lake and from river runoff, which we set as a fixed percentage of the precipitation that falls into the basin. All water loss is due to evaporation

the natural variability of lake level that occurs in response to white noise—the stochastic year-to-year fluctuations in weather that occur even without any climate change or persistence in the climate.

Other studies have sought to understand the behavior of GSL. Kite (1989) proposed that the changes and apparent periodicity in the GSL's record are within the range of normal fluctuations and are not ascribed to climatic change. Mohammed and Tarboton (2011) refer to the lake's bathymetry to explain the large and long excursions of the lake record. They note that the area of the lake controls the outgoing flux, and therefore a shallow lake like the GSL is quickly stabilized and modulated by the available evaporative surface. In subsequent work, Mohammed and Tarboton (2012) use a simple lake model to calculate the sensitivity of the GSL to changes in inflow, precipitation, and air temperature, and use variations of historical climate input to predict possible future lake-level scenarios.

Our work is similar in spirit to that of Mohammed and Tarboton (2011, 2012), but rather than being predictive, our goal is to understand the natural lake variability in order to put past and anticipated future fluctuations in context. We also extend this work by considering the role of alternate lake bathymetries on natural lake-level variability.

3 The lake-level model

In the following sections, the full and linearized models are described. The full model is similar to that of

Mason et al. (1994), who derive general and comprehensive time-dependent solutions to a lake's water balance. They explore the response of lake level and area to step changes, single brief excursions, and sinusoidal variations in the climate. In contrast, our focus here is on the lake's response to the continuous random perturbations in forcing that occur even in a constant climate. The lake model will first be presented in the context of our case study of the GSL, but will later be generalized to other lake geometries.

3.1 The full model

The rate of volumetric change for a closed-basin lake such as the GSL is determined by the balance of inflow into and evaporation out from the lake, illustrated in Fig. 4. The mass budget can be described by a straightforward differential equation:

$$\frac{dV}{dt} = PA_L + I - EA_L, \quad (1)$$

where $V_L(t)$ is the lake's volume, $A_L(t)$ is the lake's surface area, $P(t)$ is the annual regional precipitation rate, $I(t)$ is the total annual river inflow from the surrounding basin, and $E(t)$ is the annual evaporation rate over the lake, all functions of time, t .

Equation (1) can be rewritten in terms of lake-level variations. The volume of water is a unique function of lake level: $V = V(h)$, which can also be written as $V(h) = \int_0^h A_L(z) dz$. Hence

$$\frac{dV}{dt} = \frac{dV}{dh} \frac{dh}{dt} = A_L(h, t) \frac{dh}{dt}. \quad (2)$$

Substituting Eq. (2) into Eq. (1) yields:

$$\frac{dh}{dt} = \frac{1}{A_L} (PA_L + I - EA_L). \quad (3)$$

We assume that the long-term mean of the inflow, \bar{I} , is proportional to the product of the long-term mean of the annual regional precipitation rate, \bar{P} , and the area over which runoff is collected (i.e., the area of the catchment basin, excluding the direct precipitation over the lake):

$$\bar{I} = \alpha \bar{P} (A_B - \bar{A}_L), \quad (4)$$

where A_B is the entire catchment area of the lake. The parameter α reflects the fact that much of the precipitation that falls into the basin is lost to evapotranspiration or groundwater percolation. Some of the uncertainty in regional precipitation may also be subsumed into α . We set α so that the lake level matches its long-term mean. For the GSL an α of 0.13 yields an \bar{I} of $2.5 \text{ km}^3 \text{ year}^{-1}$, which is close to the values estimated from stream gauges by Arnow and Stephens (1990) ($2.3 \text{ km}^3 \text{ year}^{-1}$) and Mohammed and Tarboton (2012) ($2.8 \text{ km}^3 \text{ year}^{-1}$).

The fluctuations in inflow, I' are parametrized as

$$I' = \gamma P' (A_B - A_L), \quad (5)$$

where P' denotes the variations away from \bar{P} . If I' is negative, and its magnitude is greater than \bar{I} , the inflow is set to zero. We have introduced a tunable parameter, γ , which ensures that the interannual fluctuations in inflow are the same as observed. We find we need $\gamma = 0.40$ in order to emulate the observed standard deviation of inflow which is $\sim 1.5 \text{ km}^3 \text{ year}^{-1}$ (Mohammed and Tarboton 2012). That we require different values for α and γ suggests that there is some slow-timescale process in the region's groundwater that is neglected in our model. For the purposes of our study here, our goal is to drive the lake model with interannual variability in inflow whose magnitude is consistent with observations. Our use of γ allows us to do that.

We use the time series of P and E shown in Fig. 2b, d to force Eq. (3), using the parameter values shown in Table 1, starting in 1901 with the initial condition of $h = 1280 \text{ m a.s.l.}$, consistent with the observations. This initial lake level corresponds to a volume of 18.4 km^3 and an initial area of 4100 km^2 . From 1901 to 1956, there is no evaporation data, and so for this interval we force the lake with variations in precipitation only, keeping the evaporation rate at its long-term mean of 1 m year^{-1} . The simulated lake-level history is shown in Fig. 2a. Despite its crude treatment of inflow and incomplete evaporation record, the detrended interannual standard deviation of model lake level (1.19

Table 1 Parameters and historical values describing the GSL's lake-level and climatic history

	Variable	Historical GSL value
V_L	Lake volume	20 km^3
A_b	Catchment basin area	$5.5 \times 10^4 \text{ km}^2$
\bar{A}_l	Mean lake area	4300 km^2
σ_{A_l}	SD lake area	840 km^2
\bar{z}	Mean lake depth	10 m
\bar{h}	Mean lake level	1280.4 m a.s.l.
σ_h	SD lake level	1.14 m
\bar{P}	Mean precipitation rate	0.37 m year^{-1}
σ_P	SD precipitation rate	0.08 m year^{-1}
\bar{E}	Mean evaporation rate	1.00 m year^{-1}
σ_E	SD evaporation rate	0.10 m year^{-1}
α	% of basin's precip. flowing to lake (mean)	0.13
γ	% of basin's precip. flowing to lake (variance)	0.40
τ	e-folding time scale	8 years

See text for sources

m), agrees well with that of observations (1.14 m). The model time series correlates with observations at $r = 0.85$, which equates to a Nash-Sutcliffe model efficiency of 0.72 (Nash and Sutcliffe 1970). The fact the model does a good job in the early part of the record, despite the absence of evaporation variations suggests that the precipitation is of primary importance in driving lake-level fluctuations, a result we confirm in the next section. Consistent with this, the short period of artificial pumping (Fig. 2d) contributed only a small amount to the mass balance; this loss is folded into the evaporation term for 1986–1988.

3.2 The linear model

In the following section, we develop a linear version of the lake-level model. From it, we derive analytical solutions for the lake's relaxation timescale, the relative importance of P and E , and the variance of the lake level in response to stochastic climate forcing. The analytic expressions allow us to characterize the behavior of the lake without a complete knowledge of lake bathymetry and to clearly understand the parameters that drive the lake-level responses to climate variations.

Equation (3) is linearized by rewriting all time-varying fields using overbars to denote long-term means, and primes to denote anomalies from that mean: $P(t) \equiv \bar{P} + P'(t)$, $E(t) \equiv \bar{E} + E'(t)$, $I(t) \equiv \bar{I} + I'(t)$, $A_L(t) \equiv \bar{A}_l + A'_l(t)$, and $h(t) \equiv \bar{h} + h'(t)$.

Using Eqs. (4) and (5) for \bar{I} and I' , Eq. (3) becomes:

$$\begin{aligned} \frac{d(\bar{h} + h')}{dt} &= \frac{1}{(\bar{A}_L + A'_L)} [(\bar{P} + P')(\bar{A}_L + A'_L) \\ &+ (\alpha\bar{P} + \gamma P')(A_B - (\bar{A}_L + A'_L)) \\ &- (\bar{E} + E')(\bar{A}_L + A'_L)]. \end{aligned} \quad (6)$$

Because A_L is a function of h , we rewrite it using a first-order Taylor Series expansion:

$$A_L(h) = A_L(\bar{h} + h') = A_L(\bar{h}) + \frac{dA_L(\bar{h})}{dh} h' \equiv \bar{A}_L + \frac{d\bar{A}_L}{dh} h'. \quad (7)$$

Substituting $\frac{d\bar{A}_L}{dh} h'$ for A'_L , and considering only first-order terms, Eq. (6) becomes:

$$\frac{dh'}{dt} + \frac{h'}{\tau} = \left[1 - \gamma + \frac{\gamma A_B}{\bar{A}_L} \right] P' - E', \quad (8)$$

where

$$\tau = \frac{\bar{A}_L}{\frac{d\bar{A}_L}{dh} (\bar{E} - \bar{P}(1 - \alpha))}. \quad (9)$$

The value for τ represents the characteristic, e-folding timescale on which perturbations in lake level will relax towards the mean. A large \bar{A}_L implies that τ will also be large, because, all else being equal, for a given h' , there is a large anomalous volume, $A_L h'$, that must be either filled or evaporated to return to equilibrium. A large value of $d\bar{A}_L/dh$ is associated with smaller τ , because it means that an increase in h' leads to a large increase in evaporating area, enabling the excess volume of water to be more rapidly removed. Likewise, a decrease in h' significantly decreases the evaporating area, reducing the total evaporation, and allowing the lake to return more rapidly to equilibrium. Finally, a large difference between \bar{E} and $\bar{P}(1 - \alpha)$ indicates that the lake is in an arid region, and that the restoring tendency of E is relatively efficient. Aridity, therefore, also tends to shorten the response time of a lake. However as we discuss below, in a given setting these three factors influencing τ cannot be considered independent of each other.

The GSL is a large, shallow lake in an arid environment and so there are trade-offs between the factors that determine τ . For the values shown in Table 1, Eq. (9) predicts that $\tau = 11$ years. Our τ falls within the range of 4–17 years cited by Mason et al. (1994), who estimate several equilibrium e-folding response times for different historical levels of the GSL. Further, our value for τ compares quite well with the e-folding time suggested from observations (8 years, Fig. 3).

From Eq. (9), we see that τ is a function of the mean lake level (since \bar{A}_L and $\frac{d\bar{A}_L}{dh}$ are functions of h), and the mean

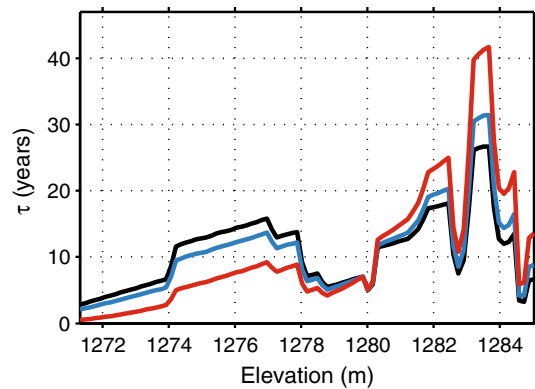


Fig. 5 The e-folding timescale of the GSL, τ , calculated from Eq. 9, for different lake-level elevations. Each \bar{h} corresponds to a specific \bar{A}_L and $\frac{d\bar{A}_L}{dh}$. The black curve holds \bar{E} and \bar{P} constant, varying only \bar{h} and its associated \bar{A}_L and $\frac{d\bar{A}_L}{dh}$ to vary. However, from Eq. (9), a change in the mean precipitation or evaporation affects τ directly, as a parameter in the equation, and indirectly, by modifying the mean area of the lake. The blue curve holds \bar{E} constant, and associates an increase (decrease) in \bar{P} with an increase (decrease) in lake level and lake area, providing a more physically consistent range of values for τ . Similarly, the red curve holds \bar{P} constant, and associates an increase (decrease) in \bar{E} with a decrease (increase) in lake level and lake area

climatic setting. τ is therefore a function of a particular mean state of the lake. The black line in Fig. 5 shows how τ varies with \bar{h} for the GSL, keeping \bar{E} , \bar{P} , and α fixed. Over the historical range of GSL lake levels (1277.5–1283.8 m a.s.l.), τ ranges from as low as 5 years at 1280 m a.s.l., to as long as 26 years at the historical high. The 5-year response time is due to a large value of $d\bar{A}_L/dh$, indicating that the basin area is changing rapidly at these elevations (evident in Fig. 1b). The 26-year response time corresponds to a large value for \bar{A}_L , as well as a relatively small value for dA_L/dh . The timescale plummets for elevations above 1284 m a.s.l., because dA_L/dh increases, allowing the lake to quickly adjust to anomalies in the water balance.

However, it is not consistent to vary \bar{h} independently, since a long-term lake-level change also requires an accompanying change in \bar{P} or \bar{E} to maintain the new mean lake level. For example, an increase in \bar{A}_L only happens if also accompanied by a decrease in \bar{E} or an increase in \bar{P} . These both work in the same direction as an increase in \bar{A}_L , acting to increase τ . Thus, it is more realistic to constrain τ through consistent combinations of \bar{h} , \bar{P} , and \bar{E} that ensure the lake is in equilibrium (i.e. $\frac{dV}{dt} = 0$ for a given \bar{h}). Figure 5 shows two examples. For the first (blue line), we vary \bar{P} keeping \bar{E} fixed, so that $\frac{dV}{dt} = 0$ in Eq. 3. For the second (red line) we vary \bar{E} , keeping \bar{P} fixed.

When the parameters covary like this, the basic pattern of the variation of response time with lake level is the same as varying \bar{h} on its own. However, confirming the reasoning

given above, the variations in τ are amplified. τ reaches 41 years for $\bar{h} = 1284$ m a.s.l., when \bar{h} and \bar{E} covary (Fig. 5).

Despite the large changes in τ as a function of \bar{h} , the linear model (Eq. 8) does a remarkably good job of emulating the historical lake level record when it is driven by the historical variations in P' and E' (Fig. 2a). The correlation with the observations is 0.83, only slightly smaller than that for the full model. The results lend confidence that we can use the linear model to derive analytical expressions for some useful metrics of the lake response.

3.2.1 Response to step changes in P and E

Let ΔE be a step-change in evaporation rate. From Eq. (8), and assuming $P' = 0$, the resulting equilibrium change in lake level (i.e., when $dh/dt = 0$) is

$$\Delta h_E = -\tau \Delta E. \quad (10)$$

Similarly, for a step-change in the precipitation rate, ΔP , the resulting change is

$$\Delta h_P = \left[1 - \gamma + \frac{\gamma A_B}{\bar{A}_L} \right] \tau \Delta P. \quad (11)$$

A simple measure of the relative importance of P and E for the lake level is the ratio of Δh_E and Δh_P :

$$R_{\Delta h} = \left| \frac{\Delta h_E}{\Delta h_P} \right| = \left| \frac{-\Delta E}{\left(1 - \gamma + \frac{\gamma A_B}{\bar{A}_L} \right) \Delta P} \right|. \quad (12)$$

In other words, $R_{\Delta h}$ is proportional to the ratio of the two climate changes, modified by the lake geometry and evapotranspiration in the catchment basin.

3.2.2 Standard deviation in lake level

As was argued in the introduction, and as was supported by an analysis of the instrumental climate record, a sensible null hypothesis is that interannual climate variability can be characterized by stochastic, normally-distributed white noise, with standard deviations in P' and E' of σ_P and σ_E respectively.

Analytical solutions for the standard deviation in lake response, σ_L , can be derived for the lake-level response to the stochastic variability from Eq. (8), and are presented in the “Appendix”. For lake-level variability driven by $E'(t)$ alone, we find

$$\sigma_{hE} = \sigma_E \sqrt{\frac{\Delta t \tau}{2}}. \quad (13)$$

Lake-level variability driven by $P'(t)$ alone is

$$\sigma_{hP} = \sigma_P \left[1 - \gamma + \frac{\gamma A_B}{\bar{A}_L} \right] \sqrt{\frac{\Delta t \tau}{2}}. \quad (14)$$

Combining Eqs. (13) and (14), we get:

$$\sigma_h^2 = \sigma_{hE}^2 + \sigma_{hP}^2. \quad (15)$$

For the GSL, $\sigma_{hP} = 1.04$ m, $\sigma_{hE} = 0.24$ m, and $\sigma_h = 1.07$ m, meaning that P' contributes 95 % of the variance in fluctuations in h' . This confirms our earlier result (Fig. 2a), that lake level fluctuations in the GSL are predominantly driven by precipitation variability. A more comprehensive study of lake geometry and climatic conditions would be needed to establish whether this is generally true, or whether under some conditions evaporation variability dominates. The predominant importance of precipitation and inflow for the GSL is also noted by Mohammed and Tarboton (2012). The dominance of precipitation has also been shown for East African lakes (Hastenrath and Kutzbach 1983), and is therefore not unique to the GSL.

Finally, although we have assumed normally distributed white noise in agreement with observations, we note that it would be possible to incorporate skewness or higher statistical moments into the forcing distributions. At least for the linear model the shape of the probability distribution function (PDF) of the climate forcing is directly transferred into the shape of the PDF in the lake-level response.

4 Statistics of long-term variability for the Great Salt Lake

To this point, we have demonstrated that both the full and linear models can capture the general behavior of the GSL's historical lake-level variations. We now turn to characterizing the lake's behavior beyond the historical record: its variance; power spectrum; lake-level threshold-crossing probabilities; and evaluating the analytical expressions derived from the linear model, when forced with stochastic climate variations. The differences between the models highlight the capacity of the analytic solutions to describe the behavior of the lake, and the degree to which changes in the geometry of the lake basin and bathymetry are important.

We force the full and linear models with long (10^6 year) realizations of $P'(t)$ and $E'(t)$ generated from normally distributed, white-noise processes that have the same mean and variance as the observations (detailed in Table 1). A 300-year snapshot of the resulting lake-level time series is shown in Fig. 6a, with the full model in grey, and the linear model in blue. The full time series correlate highly with one another ($r = 0.89$), but there are also notable differences. For example, because the full model resolves changes in $\frac{dA_L}{dh}$, which decreases below the present lake level, the full model's response time is longer at lake levels just slightly lower than the mean lake level. Therefore, the full model's lake level is consistently lower than that of the linear.

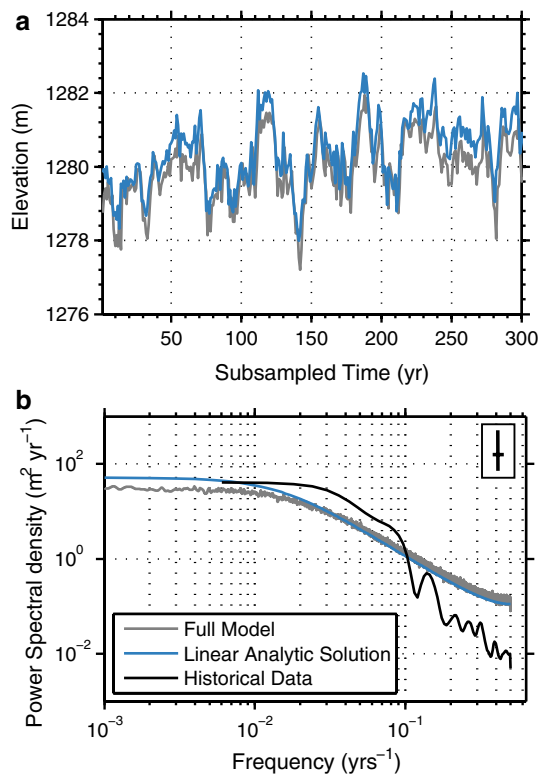


Fig. 6 Long-term climate statistics. **a** A 300-year time slice of the full (grey) and linear (blue) lake-level model output, forced by stochastic variations in precipitation and evaporation. The two models are highly correlated ($r = 0.89$). **b** The power spectra of the models and historical data (in black). The linear curve is calculated following Box et al. (2013). The full model's spectrum was computed with a Hanning Window length of ten-thousand, with no overlap between the windows. The historical data's error bar is shown in the top right corner, with the horizontal line marking the intersection with the curve. Because full model was run for a million time steps, its error is negligible. The models capture variability well on timescales of decades or longer, but overestimate the variability at higher frequencies

4.1 Standard deviations

For the full model, we find $\sigma_h = 1.0$ m, in close agreement with the linear model ($\sigma_h = 1.1$ m). The PDFs are shown in Fig. 7a. The PDF of the lake levels for the linear model is normal by construction, but the actual hypsometry of the GSL introduces a significant degree of skewness in the full model (skewness = -0.2 ; kurtosis = 3.4). Therefore, the full model is not consistent with a normal distribution (at $p = 0.05$, based on a Kolmogorov-Smirnov test [e.g. von Storch and Zwiers 2001]).

Relative to the mean, the full model's lake-area extremes are skewed towards negative excursions (Fig. 7b). The area that is associated with $+3\sigma_h$ is 6000 km^2 , and covers about 2.5 times the area associated with $-3\sigma_h$, 2300 km^2 (Fig. 7c, d). This range is comparable to the difference between the highest and lowest areas in the historical record, and

describe the expected extremes seen in a thousand-year period, if there was no climatic change.

4.2 Power spectral density

The power spectra of lake level for the models and the historical record are shown in Fig. 6b. The spectrum for the linear model is calculated using a standard formula for Eq. (8) (e.g. Box et al. 2013), which applies to frequencies $0 \leq f \leq \frac{1}{2\Delta t}$:

$$\mathcal{P}(f) = \frac{\mathcal{P}_0 \left(\frac{\Delta t}{\tau}\right)^2}{1 - 2\left(1 - \frac{\Delta t}{\tau}\right) \cos(2\pi f \Delta t) + \left(1 - \frac{\Delta t}{\tau}\right)^2}, \quad (16)$$

where $\mathcal{P}(f)$ is the power spectral density, $\mathcal{P}_0 = 4\tau\sigma_h^2$, and σ_h is taken from the linearized model (i.e., Eq. 15).

The area beneath the power spectrum is the variance of the time series, and so the similarity of the power spectra of the full and linear models is consistent with their values for σ_h also being similar. There are however some noteworthy differences between the models and the observations. While the spectral power at low frequencies is quite similar, the observations are more damped than the models at high frequencies.

The power spectrum is the Fourier transform of the autocorrelation function (e.g. Box et al. 2013). Therefore the extra damping at high frequencies in observations above that predicted by Eq. (16) is consistent with the observed autocorrelations at short lags being higher than predicted by a simple exponential function (Fig. 3). Similar behavior was found recently for the glaciers by Roe and Baker (2014).

For the GSL, these results suggests that neither Eq. (3) nor Eq. (8) are complete descriptions of the lake response. In particular, groundwater dynamics likely impacts lake-level variability at higher frequencies. Further development of the model might better emulate the observed autocorrelation/power spectrum structure. These differences notwithstanding, the results confirm the basic principle embodied in the models. For the historical record, persistence in lake level fluctuations is associated with the memory of the lake system, rather than persistence in climate.

4.3 Threshold crossing statistics

Often it is the extrema of lake level (i.e. a flood or extreme lowering) that have the highest impacts on water resources and are most evident in proxy records. A metric of particular importance then, is the likelihood that a given lake level is reached in a given period of time. Given interannual climate variability, the question is inherently a statistical one. For the full model, the statistics can be estimated

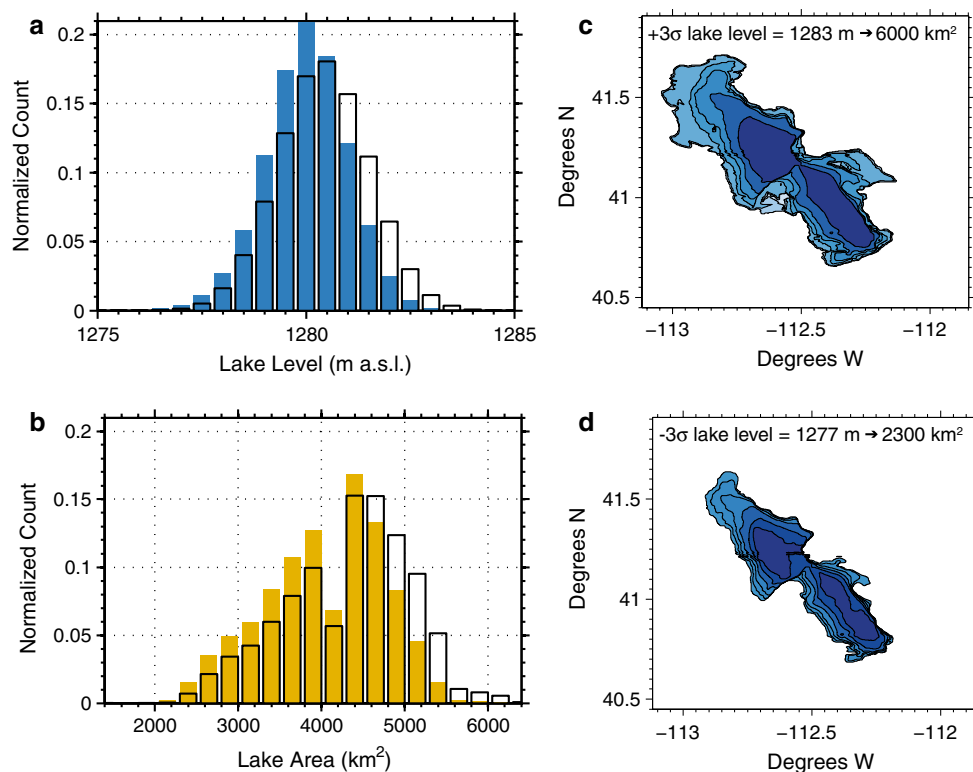


Fig. 7 The distribution of lake level (**a**) and lake area (**b**) for the long-term forcing experiments. The linear model is outlined in *black*, and full model is represented with the *bars* that are filled in. Only the

linear lake-level model output is normally distributed. **c** and **d** The areas associated with $\pm 3\sigma_h$ for the full model run

from the long idealized simulations of lake level. For the linear model, the statistics can be derived analytically from the statistics of a Poisson distribution (e.g. von Storch and Zwiers 2001; Roe 2011). The probability of the lake level exceeding a given threshold, h_0 , above or below the long-term average at least once in a given interval of time, $t_f - t_i$, is given by:

$$p(N(t_f - t_i) \geq 1) = 1 - \exp\left[-\frac{t_f - t_i}{2\pi} \left(\frac{2}{\tau \Delta t}\right)^{\frac{1}{2}} e^{-\frac{1}{2}\left(\frac{h_0}{\sigma_h}\right)^2}\right]. \quad (17)$$

Equation (17) shows that the longer the time interval ($t_f - t_i$), the higher the probability of exceeding a given threshold. This probability depends on τ , but is especially sensitive to the ratio of h_0 and σ_h .

Figure 8a shows results for time intervals of 100, 500, and 1000 years. For the full model we randomly sample these intervals 10^5 times from the long model integration, and collate the statistics of how often a given lake level is crossed. As an example, for the full model, in any 1000 years period it is extremely likely (98 %) to find the lake level exceeding 2 m above the average, and extremely unlikely (<1 %) to find the lake level exceeding 4 m above the average.

The threshold-crossing probability curves show that the full and linear models diverge at the extremes. For the linear model, the maxima and minima curves are symmetric about the mean lake level, as expected from the probability distribution function of the lake levels (Fig. 7a). However, for the full model, a large lake-level minimum is more likely than a lake-level maximum of the same magnitude. This is also apparent in Fig. 6a, where the full model's lake levels are consistently lower than those of the linear model, and in (Fig. 6b), which shows differences between the spectra of each model. Though the standard deviations of the models are quite close, the linear model overestimates the frequency of a lake-level maximum and underestimates the frequency of a lake-level minimum, relative to the full model.

Figure 8b shows the full model's frequency-crossing distribution for the total excursion of a given time slice (i.e. the (maximum–minimum) values within $(t_f - t_i)$). This illustrates total expected spread in the lake level on the order of 100, 500, or 1000 years. The GSL has a higher than 50 % probability of varying more than 4 m within a century; more than 5.5 m every 500 years; and more than 6 m every millennium. Interestingly, Karl and Young (1986) inspected the return times for precipitation records

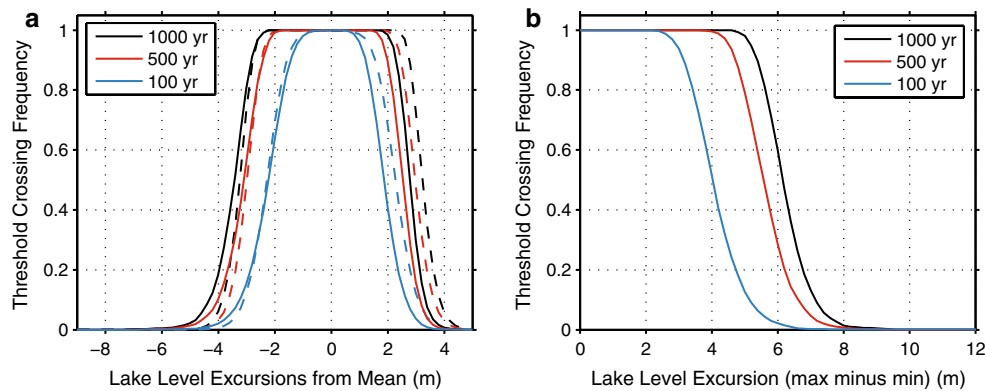


Fig. 8 a The maximum and minimum lake-level excursions from the mean for random 1000, 500, and 100 year time-slices within the long-term model runs. The *solid lines* show the probability of a given excursion for the full model, while the *dashed lines* show the analytic

solutions to the linear model. The *dashed lines* are symmetric about zero, while the *solid lines*' asymmetry reflects the effect of the lake's varying hypsometry. **b** The total excursion probability in a given 1000, 500, and 100 year time-slices of the full model

alone, and found that there was greater than 50 % probability of having a wet spell as extreme as the 1986 floods in any hundred year period, with a return time of 120 years. The similarity between the high precipitation probability and flood probability is unsurprising, given how sensitive the lake is to changes in precipitation.

5 Statistics of long-term variability for alternative lake hypsometries

We have focused on the GSL because of its long lake-level history, relatively short response time, and detailed hypsometric information. However, the framework developed above can be used to characterize any closed-basin lake's response to variations in the climate. This response will be dependent on the lake's unique hypsometry and regional climate.

To understand the extent of geometric influence on the timescale and magnitude of lake-level variability, we create simple hypsometric profiles that are approximations to the bathymetry of three closed-basin lakes: the extensive and shallow GSL; the extensive and deep Lake Titicaca, on the border of Bolivia and Peru; and the areally small and deep Lake Bosumtwi in Ghana (Fig. 9a–c). In the following calculations we do not try to simulate historical or projected future variations of these lakes, but aim to isolate the impact of different lake geometries on lake-level response. The simple functions used to describe the bathymetry allow $d\bar{A}_L/dh$ to vary smoothly, in turn, smoothing the lake-level response.

The GSL and Lake Titicaca's hypsometric curves are concave down, and can be idealized as an inverted rectangular pyramidal frustum:

$$A_L(h) = LW \left(\frac{h + z_0}{z_0 + z_1} \right)^2, \quad (18)$$

where, again, A_L is the lake area and h is the lake level. L and W are the length and width of the basin at some known elevation, z_1 , above the bottom of the frustum, and z_0 is the vertical distance from the bottom of the frustum to the point that would complete a full pyramid.

Lake Bosumtwi's hypsometric curve is concave up, and is idealized as a tri-axial half-ellipsoid:

$$A_L(h) = \pi LW \left(1 - \frac{(z_0 - h)^2}{z_0^2} \right), \quad (19)$$

where L , W and z_0 are the lengths of the semi-principal x , y , and z axes, and $h = 0$ at $z = z_0$. The values for each lake's parameters are given in Table 2, and are compared with the known hypsometric profiles in Fig. 9.

Estimates for \bar{E} and \bar{P} for lakes Titicaca and Bosumtwi are available from the literature [Table 2, Turner et al. (1996); Richerson et al. 1977]. For each idealized lake geometry, we set α so as to match the modern lake levels. By analogy with the GSL, we set $\gamma = 3\alpha$.

In order to focus solely on the impact of the different basin geometries on lake-level variability, we apply the same $E'(t)$ and $P'(t)$ to all three idealized lake geometries as were applied to the GSL (see Sect. 4). We integrate the full lake model (Eq. 3) with each of the idealized lake geometries, and use the linear model solutions to calculate τ , σ_h , and $\mathcal{P}(f)$ for each lake. All parameters are provided in Table 2.

A 2000-year slice of each lake's time series is shown in Fig. 9d. It is clear that the lakes respond to the same perturbations at different timescales and with different amplitudes. The analytic solutions to the linear model allow us to link the differences in lake response to each lake's parameter values.

Fig. 9 Alternative geometry experiments. The simplified geometries (a frustum or half-ellipsoid, shown in *color*) for the Great Salt Lake (a) Lake Titicaca (b), and Lake Bosumtwi (c), over their hypsometric curves (shown in *black*). The hypsometric curves are interpolated from Turner et al. (1996) (Bosumtwi) and Richerson et al. (1977) (Titicaca). The crosses mark the present-day lake levels for each of the lakes. d A 2000-year time slice from the long-term alternative lake model runs, showing the diverging behavior of the three lakes. e The power spectra of the lakes. The full models are noisier, while the analytic solutions to the linear model are overlain above

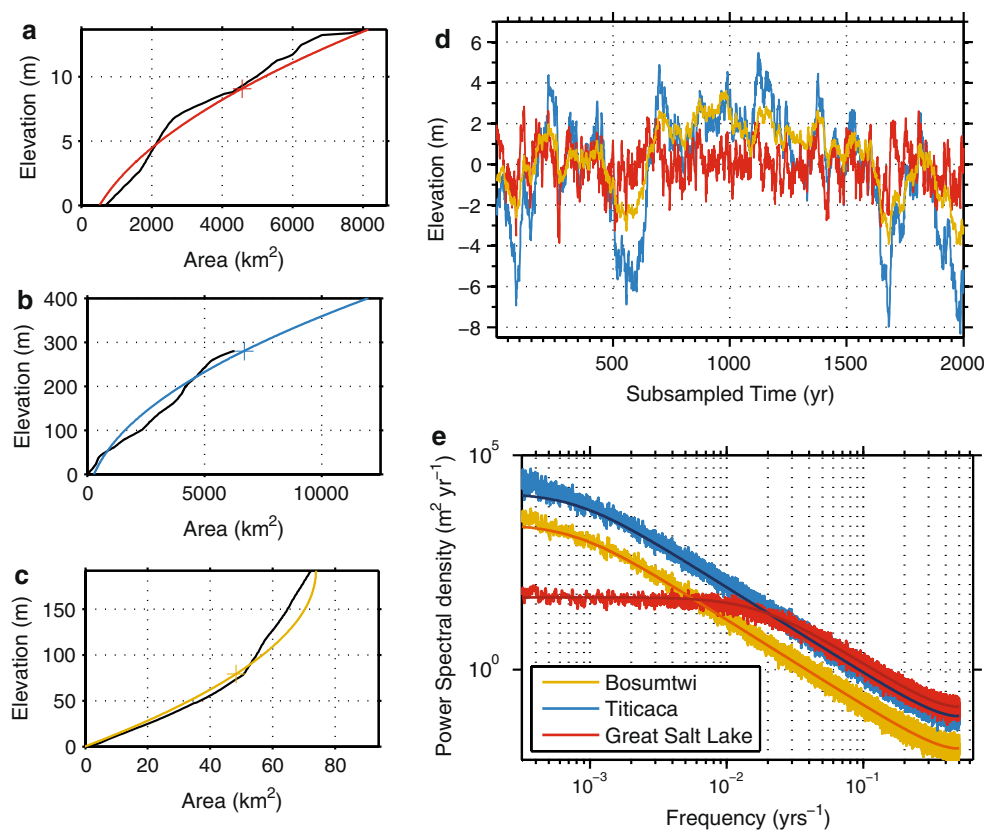


Table 2 Parameters, and model outputs for the simplified geometry experiments

	GSL	Bosumtwi	Titicaca	
z	14	192	400	m
L	150	5	150	km
W	50	4.7	80	km
A_b	55,000	72	58,000	km ²
\bar{A}_L	4600	48	6700	km ²
$d\bar{A}_L/dh$	665	0.45	38	km ² m ⁻¹
\bar{h}	9	79	280	m
σ_h	1.1	1.7	4.0	m
\bar{P}	0.37	1.38	0.80	m year ⁻¹
σ_P	0.08	0.08	0.08	m year ⁻¹
\bar{E}	1.0	1.55	1.58	m year ⁻¹
σ_E	0.1	0.1	0.1	m year ⁻¹
α	0.16	0.25	0.13	–
γ	0.47	0.75	0.38	–
τ	10	209	201	year

Lake Bosumtwi's climate variables are from Turner et al. (1996), and Lake Titicaca's are from Richerson et al. (1977). σ_P and σ_E for all three lakes are, by experimental design, equal to the GSL's: these numbers are inaccurate, and should not be used in other studies

5.1 Response time

The response time for each lake is calculated using Eq. (9). The idealized GSL has the fastest response time, with a $\tau = 10$ years, because of its large $d\bar{A}_L/dh$. The shape of Lake Bosumtwi is very different, with a relatively small area of 48 km², but a modern depth of 79 m. Its geometry means that if Lake Bosumtwi experiences a brief increase in P , the lake level will increase, but the lake's surface area only increases slightly. Hence, it takes many years for a steady \bar{E} to remove the excess water and return the lake to its original level. Therefore, though the surface area of Lake Bosumtwi is much smaller than that of Lake Titicaca or the GSL, its small $d\bar{A}_L/dh$ gives the lake a long memory, with an e-folding time of 209 years. Lake Titicaca is much larger ($\bar{A}_L = 6700$ km²) and deeper ($\bar{h} = 280$) than the GSL or Lake Bosumtwi. However, Lake Titicaca's ratio of $\bar{A}_L : d\bar{A}_L/dh$, and therefore its τ (=201 years), is similar to that of Lake Bosumtwi.

The mean climatic differences (\bar{P}, \bar{E}) also affect τ , as does the ratio of \bar{A}_L and A_b , through the α needed to

maintain the modern lake level. These effects are, however, of secondary importance to the basin hypsometry.

The hypsometry of the lake, then, is the main control over the response time of the lake, which, in turn, determines the integration of the climatic history in the lake-level record.

5.2 Standard deviations

For the idealized GSL geometry, $\sigma_h = 1.1$ m for both the full and models, which is very similar to the values for the original model runs. Lake Bosumtwi's σ_h is comparable, with $\sigma_h = 1.7$ m for both models. The reason that σ_h is similar for Lake Bosumtwi and the GSL is because τ and basin geometry compensate one another (Eq. 15): while τ is much larger for Bosumtwi than the GSL, the ratio of A_B/\bar{A}_L is much smaller. Lake Titicaca, with a large values for both τ and A_B/\bar{A}_L , exhibits the largest values for $\sigma_h = 4.0$ m for both models.

5.3 Power spectrum

Figure 9e shows the lake-level power spectra for each of the three lakes. The $\mathcal{P}(f)$ s from Eq. (16) are also shown. The GSL has more power at high frequencies than Lake Bosumtwi or Lake Titicaca, with their long response times. Lake Bosumtwi and Lake Titicaca, which have similar values for τ , have similar spectral shapes, though Titicaca has more power at all frequencies, simply because its variance is greater. The smaller τ and lower overall variance for GSL means that it asymptotes more rapidly and to a lower value of $\mathcal{P}(f)$ at low frequencies.

Mason et al. (1994) show that the high-frequency component of lake-level variability is proportional to $\bar{E} - \bar{P}$ and the ratio of \bar{A}_L to A_B , while the low-frequency component is proportional to τ , $\bar{E} - \bar{P}$, and the ratio of \bar{A}_L to A_B . Our findings corroborate this, since Titicaca and Bosumtwi, with their similar values for τ have spectra that diverge from the GSL's at low frequencies. Similarly, the spectra of the GSL and Titicaca are more similar at high frequencies, because their $\bar{E} - \bar{P}$, and the ratio of \bar{A}_L to A_B are more comparable.

6 Summary and discussion

In this study we have sought to characterize and understand the response of lake level and lake area to the year-to-year fluctuations in precipitation and evaporation that are intrinsic to a constant climate. We have focussed especially on the case study of the Great Salt Lake (GSL), because of the availability of long

observational records of inflow, evaporation, and lake level, and because of an extensive literature on GSL (e.g. Mann et al. 1995; Abarbanel et al. 1996; Lall et al. 1996; Loving et al. 2000; Mohammed and Tarboton 2011, 2012). From the available meteorological and hydrological observations, we showed that the climate variability that drives GSL lake level is mostly consistent with normally-distributed white noise, the exception being that slight interannual persistence was indicated for precipitation. It is well established that lakes have an intrinsic response time, or memory, that is a function of their geometry, hydrology, and climatic setting (e.g. Mason et al. 1994). A robust effect of this response time is that a lake will integrate the year-to-year climate fluctuations to produce persistent (multi-decadal to centennial) fluctuations in lake level (Fig. 9). The effect of a system's memory in producing persistence (or 'reddening') in the response is well known in other areas of climate science (e.g. Hasselmann 1976; Oerlemans 2000) but to our knowledge has not been applied to the interpretations of past lake-level fluctuations.

We used both full water-balance and linear lake models calibrated to observations of the GSL, and showed that the historical (160 years) record of GSL lake level is largely consistent with the expected lake-level statistics driven simply by the stochastic year-to-year climate fluctuations observed in the modern instrumental record. Therefore we conclude that interannual climate variability has likely been an important driver of lake-level fluctuations in recent millennia (e.g. Atwood 1994; Atwood and Mabey 2000).

While the lake models accurately capture the low-frequency response of the historical record of the GSL, they both overestimate the high frequency response, suggesting that not everything in the lake-level response is captured. A more detailed analysis of the autocorrelation structure using auto-regressive moving-average (ARMA) modeling might reveal higher-order terms in the lake response. This approach was recently used by Roe and Baker (2014) to analyze glacier response. A likely source of additional damping at high frequencies is groundwater percolation, and adapting the model to account for it would be a useful next step.

The linear lake-level model performed comparably well to the full model, and it provides some useful analytic expressions for some important metrics of lake-level sensitivity: response time, relative importance of precipitation and evaporation, lake-level variance, power spectrum, and the expected return time of lake-level high stands. This last metric is particularly useful for evaluating the significance of past lake-level fluctuations and, to our knowledge, is new to the lake literature.

The dependencies of these useful statistical metrics on geometry and climatic setting are transparent. For many purposes the linear model may be the best approach: uncertainties in climatic forcing and evapotranspiration are likely to be larger source of error in modeling lake response than the model itself. Thus, a more complicated model may not be justified for characterizing the response to interannual variations in climate.

However, one important difference between the full and linear models is that the linear model has a normally distributed lake-level PDF because it is linear and because the climate variability PDF was assumed normal, consistent with observations. It does not capture the negative skewness of the full model's lake-level PDF (Fig. 7a), which arises from changes in the lake hypsometry slope as a function of lake level (i.e., Figs. 1b, 9a–c). The PDFs of area for both models are non-normal because of the lake hypsometry. Thus, it is important to evaluate the possible impact of changing hypsometry when characterizing the behavior of lake response.

Our case study of the GSL established the robust principle that persistent lake-level fluctuations will occur even in a climate with no persistence. We then repeated our modeling exercises on idealized bathymetries of the GSL, Lake Titicaca, and Lake Bosumtwi, in order to isolate the effect of geometry. We found a remarkable range of time scales are implicated: from ten years for the GSL to ~200 years for Titicaca and Bosumtwi. The differences can be attributed to the specific parameters that set τ and σ_h . The timescale is proportional to the lake's area, and is inversely proportional to its aridity and dA_L/dh . The amplitude of variations is a function of τ , but it is also modified by the ratio of the basin area to the lake area. Idealized geometries, such as the frustum and half-ellipsoid, and linear models are an efficient way of characterizing uncertainty analyses when working with lakes whose bathymetry is not well characterized, when analyzing many lakes, or for preliminary field-work plans.

Finally, while our main emphasis has been on building tools for interpreting past lake-level changes, there are implications for predictions of future changes. In essence we have sought to characterize a lake's natural variability—that is, the lake-level fluctuations that occur in a constant climate (i.e., absent any external climate forcing normally considered as changes in CO₂, volcanoes, solar output). The magnitude of this natural variability essentially sets the irreducible lower bound on the predictability of the future (e.g. Hawkins and Sutton 2009; Deser et al. 2012). Our estimates and models can be used as a guide for that lower bound, but should only applied with caution: changing groundwater and land usage, changing PDFs of precipitation and drought, and changing lake hypsometry as a function of mean lake-level are all important factors to consider.

Acknowledgments University of Delaware air temperature and precipitation data provided by the NOAA/OAR/ESRL PSD, Boulder, Colorado, USA, from their website at <http://www.esrl.noaa.gov/psd/>. KMH is grateful to Harvard University's Earth and Planetary Sciences Department, for providing a space to write. The authors thank the Western Regional Climate Center for providing unpublished pan-evaporation data. The authors are grateful to three anonymous reviewers for constructive and helpful comments, and to the editor, Dr. Ed Schneider.

Appendix: Standard deviations in lake level

Discretizing Eq. (8) in to time increments, Δt , and setting $P' = 0$, gives

$$h'_t = h'_{t-\Delta t} \left(1 - \frac{\Delta t}{\tau} \right) E'_t. \quad (20)$$

We set $E'_t = \sigma_E v_t$, where v_t is a normally distributed, stochastic white noise process. The variance of h'_t is the expected value of h'^2_t , and is given by

$$\begin{aligned} \langle h'^2_t \rangle &= \left(1 - \frac{\Delta t}{\tau} \right)^2 \langle h'^2_{t-1} \rangle \\ &\quad + 2 \left(1 - \frac{\Delta t}{\tau} \right) \sigma_E \Delta t \langle h'_{t-1} v_t \rangle + \sigma_E^2 \Delta t^2 \langle v_t^2 \rangle. \end{aligned} \quad (21)$$

The following relationships hold: $\langle v_t h'_t \rangle = 0$, $\langle h'^2_t \rangle = \langle h'^2_{t-1} \rangle$, and $\langle v_t^2 \rangle = 1$. Upon substitution, and taking the limit of $\Delta t \ll \tau$ we obtain:

$$\langle h'^2_t \rangle = \frac{\sigma_E^2 \Delta t^2}{2 \Delta t / \tau}, \quad (22)$$

Therefore,

$$\sigma_{hE} = \sigma_E \left(\frac{\Delta t \tau}{2} \right). \quad (23)$$

Similarly for lake-level variability due to $P'(t)$ alone:

$$\sigma_{hP} = \left[1 - \gamma + \frac{\gamma A_B}{A_L} \right] \sigma_P \left(\frac{\Delta t \tau}{2} \right). \quad (24)$$

Provided that P' and E' are not correlated the variances can be combined as:

$$\sigma_h = \sqrt{\sigma_{hE}^2 + \sigma_{hP}^2} \quad (25)$$

References

- Abarbanel HD, Lall U (1996) Nonlinear dynamics of the Great Salt Lake: system identification and prediction. *Clim Dyn* 12(4):287–297
- Abarbanel HD, Lall U, Moon YI, Mann ME, Sangoyomi T (1996) Nonlinear dynamics and the Great Salt Lake: a predictable indicator of regional climate. *Energy* 21(7):655–665

- Arnou T (1985) Water-level and water-quality changes in Great Salt Lake, Utah, 1843–1985. US Geological Survey Circular 913
- Arnou T, Stephens DW (1990) Hydrologic characteristics of the Great Salt Lake, Utah, 1847–1986. US Geological Survey Water-Supply Paper 2332
- Atwood G (1994) Geomorphology applied to flooding problems of closed-basin lakes... specifically Great Salt Lake, Utah. *Geomorphology* 10(1):197–219
- Atwood G, Mabey DR (2000) Shorelines of antelope Island as evidence of fluctuations of the level of Great Salt Lake. In: King JK, Willis GC (eds) *The geology of antelope Island, Davis County, Utah*, Utah Geological Survey
- Bartlein P, Bengtsson L, Harrison S, Hostetler S, Hsü K, Qin B, Vassiljev J (1998) Modelling lake behaviour: how can we use mechanistic models to further our understanding of the response of lakes to climate change? *Paläoklimaforschung* 25:169–177
- Baskin RL (2005) Calculation of area and volume for the south part of Great Salt Lake, Utah. US Geological Survey Open-File Report 20051327
- Baskin RL (2006) Calculation of area and volume for the north part of Great Salt Lake, Utah. US Geological Survey Open-File Report 20061359
- Box GE, Jenkins GM, Reinsel GC (2013) *Time series analysis: forecasting and control*, 4th edn. Wiley, London
- Burke EE, Roe GH (2014) The absence of memory in the climatic forcing of glaciers. *Clim Dyn* 42(5–6):1335–1346
- Deser C, Phillips A, Bourdette V, Teng H (2012) Uncertainty in climate change projections: the role of internal variability. *Clim Dyn* 38(3–4):527–546
- Frankignoul C, Hasselmann K (1977) Stochastic climate models, part II: application to sea-surface temperature anomalies and thermocline variability. *Tellus* 29(4):289–305
- Hasselmann K (1976) Stochastic climate models part I: theory. *Tellus* 28(6):473–485
- Hastenrath S, Kutzbach JE (1983) Paleoclimatic estimates from water and energy budgets of East African lakes. *Quat Res* 19(2):141–153
- Hawkins E, Sutton R (2009) The potential to narrow uncertainty in regional climate predictions. *Bull Am Meteorol Soc* 90(8):1095–1107
- Karl TR, Young PJ (1986) Recent heavy precipitation in the vicinity of the Great Salt Lake: just how unusual? *J Clim Appl Meteorol* 25(3):353–363
- Kite G (1989) Use of time series analysis to detect climatic change. *J Hydrol* 111(1):259–279
- Kohfeld KE, Harrison SP (2000) How well can we simulate past climates? Evaluating the models using global palaeoenvironmental datasets. *Quat Sci Rev* 19(1):321–346
- Lall U, Mann M (1995) The Great Salt Lake: a barometer of low-frequency climatic variability. *Water Resour Res* 31(10):2503–2515
- Lall U, Sangoyomi T, Abarbanel HD (1996) Nonlinear dynamics of the Great Salt Lake: nonparametric short-term forecasting. *Water Resour Res* 32(4):975–985
- Langbein WB (1961) The salinity and hydrology of closed lakes. US Geological Survey Professional Paper 412
- Liu G, Schwartz FW (2014) On modeling the paleohydrologic response of closed-basin lakes to fluctuations in climate: methods, applications, and implications. *Water Resour Res* 50(4):2975–2992
- Loving BL, Waddell KM, Miller CW (2000) Water and salt balance of Great Salt Lake, Utah, and simulation of water and salt movement through the causeway, 1987–1998. US Geological Survey Water-Resources Investigations Report 00-4221
- Mann ME, Lall U, Saltzman B (1995) Decadal-to-centennial-scale climate variability: insights into the rise and fall of the Great Salt Lake. *Geophys Res Lett* 22(8):937–940
- Mason I, Guzkowska M, Rapley C, Street-Perrott F (1994) The response of lake levels and areas to climatic change. *Clim Change* 27(2):161–197
- Matsuura K, Willmott C (2012) Terrestrial precipitation: 1900–2010 gridded monthly time series v 3.01. <http://www.esrl.noaa.gov/psd/>
- Mohammed IN, Tarboton DG (2011) On the interaction between bathymetry and climate in the system dynamics and preferred levels of the Great Salt Lake. *Water Resour Res* 47(2):W02525
- Mohammed IN, Tarboton DG (2012) An examination of the sensitivity of the Great Salt Lake to changes in inputs. *Water Resour Res* 48(11):W11511
- Moon Y, Lall U, Kwon HH et al (2008) Non-parametric short-term forecasts of the Great Salt Lake using atmospheric indices. *Int J Climatol* 28(3):361–370
- Morton FI (1986) Practical estimates of lake evaporation. *J Clim Appl Meteorol* 25(3):371–387
- Nash JE, Sutcliffe JV (1970) River flow forecasting through conceptual models part I: a discussion of principles. *J Hydrol* 10(3):282–290
- Oerlemans J (2000) Holocene glacier fluctuations: is the current rate of retreat exceptional? *Ann Glaciol* 31(1):39–44
- Richerson PJ, Widmer C, Kittel T, et al (1977) *Limnology of Lake Titicaca (Peru-Bolivia)*, a large, high altitude tropical lake. In: Institute of Ecology Publication, vol. 14, Institute of Ecology
- Roe GH (2011) What do glaciers tell us about climate variability and climate change? *J Glaciol* 57(203):567–578
- Roe GH, Baker MB (2014) Glacier response to climate perturbations: an accurate linear geometric model. *J Glaciol* 60(222):670–684
- Roe GH, O'Neal MA (2009) The response of glaciers to intrinsic climate variability: observations and models of late-Holocene variations in the Pacific Northwest. *J Glaciol* 55(193):839–854
- Sangoyomi TB, Lall U, Abarbanel HD (1996) Nonlinear dynamics of the Great Salt Lake: dimension estimation. *Water Resour Res* 32(1):149–159
- Sene K (1998) Effect of variations in net basin supply on lake levels and outflows. *Hydrol Process* 12(4):559–573
- Street-Perrott F, Harrison SP (1985) Lake levels and climate reconstruction. In: *Paleoclimate analysis and modeling* pp 291–340
- Turner BF, Gardner L, Sharp W (1996) The hydrology of Lake Bosumtwi, a climate-sensitive lake in Ghana, West Africa. *J Hydrol* 183(3):243–261
- USGS Water Resources (2013) Great Salt Lake at State Park Saltair Beach Boat Harbor, Utah. <http://waterdata.usgs.gov/ut/nwis/uv/>
- Von Storch H, Zwiers FW (2001) *Statistical analysis in climate research*. Cambridge University Press, Cambridge
- Waddell KM, Barton J (1980) Estimated inflow and evaporation for Great Salt Lake, Utah, 1931–1976, with revised model for evaluating the effects of dikes on the water and salt balance of the lake. Division of Water Resources, Utah Department of Natural Resources
- Wang SY, Gillies RR, Jin J, Hipps LE (2010) Coherence between the Great Salt Lake level and the Pacific quasi-decadal oscillation. *J Clim* 23(8):2161–2177
- Western Regional Climate Center (2013) Evaporation stations. <http://www.wrcc.dri.edu/htmlfiles/westevap.final.html>, time series accessed through personal communication, 01-10-14
- Willmott C, Matsuura K, Legates D (2012) Terrestrial air temperature: 1900–2010 gridded monthly time series v 3.01. <http://www.esrl.noaa.gov/psd/>